Numerical Simulation of Breaking Gravity Waves below a Critical Level

ANDREAS DÖRNBRACK and ULRICH SCHUMANN
DLR, Institute of Atmospheric Physics
D-82230 Oberpfaffenhofen, Germany

Abstract. The interaction of an internal gravity wave with a critical layer and the generation of turbulence are studied by three-dimensional numerical simulations. Based on a successful comparison of a two-dimensional version of the model with experimental observations (Thorpe, 1981), we discuss results obtained with two different models of viscosity. Although the variances of the turbulent quantities are nearly the same, a direct numerical simulation gives a smooth breaking with stable vortices. The motion remains two-dimensional. In a large-eddy simulation, the initial field is randomly disturbed and a turbulent viscosity (function of the local shear and Richardson number) is used. The breakdown of the convectively unstable regions occurs immediately after the appearance of convective instability, and small-scale three-dimensional turbulent motion is generated.

Introduction

The generation of turbulence by overturning of internal gravity waves is an important factor in the microscale dynamics of the atmosphere and ocean. For instance, the overturning of internal gravity waves and the resulting turbulence are thought to be the primary cause for clear-air turbulence [9] and for the occurrence of thin turbulent layers in the free atmosphere [10, 6, 11]. For weak stratification ($Ri < 0.25$) the turbulence may be generated by shear instability. Some theories and numerical attempts exist to explain how overturning waves are excited, however it is not known how these waves break in detail.

One of the fundamental mechanisms that lead to the breaking of gravity waves and production of turbulence is the interaction of an internal gravity wave with a critical level. In a shear flow, a critical level is the height where the phase speed of a wave equals the mean flow speed [1]. As a propagating wave approaches its critical level, the wave propagation is strongly modified: waves above the critical level decay (the trapping effect of the critical layer). In the critical layer, all momentum of the wave is transferred into the mean motion. Depending on the excitation energy of the initial wave field, shear and stratification of the basic flow, turbulence can be generated.

The gravity-wave critical-layer interaction is difficult to study observationally in the free atmosphere because of the broad spectrum of scales which prevents the observation of isolated events. In the planetary boundary layer some attempts have been made to demonstrate the critical layer effect [8, 5]. In the laboratory, the interaction has been observed under controlled conditions by defining one wavelength and prescribing a mean velocity profile. So far, only a few (mostly qualitative) observations are known [13, 3, 2].

P.R. Voke et al. (eds.), Direct and Large-Eddy Simulation I, 189–199.

Thorpe [13] used a simple experimental device: a long rectangular tube, filled with a stably stratified fluid. The lower boundary has sinusoidal corrugations of amplitude δ and wavelength λ which excite internal gravity waves with zero phase speed in the stratified shear flow. The shear flow with zero mean is forced by tilting the tube horizontally by a small angle. Its strength depends on this angle and the time of tilting. As in other experiments, no wavy motion could be observed above the critical layer. Near the critical layer the vertical propagation of the internal gravity waves was stopped and regions of reduced density gradients develop over the troughs of the surface waves. These regions become gravitationally unstable (Kelvin-Helmholtz instability is not observed).

In this paper, we present results of three-dimensional numerical simulations of the interaction of vertically propagating gravity waves with a critical layer. Two different regimes can be identified. For a smooth breaking, we use a direct numerical simulation (DNS) with constant viscosity. The mixing occurs due to a continuous rolling-up of density surfaces. In the large-eddy simulation (LES), the initial field is randomly disturbed and a turbulent viscosity is used. The breakdown of the convectively unstable regions occurs immediately after the appearance of instability and small-scale turbulent motion is generated.

Section 2 introduces the numerical model. The comparison with the experimental results of Thorpe [13] for a shear flow with zero mean is presented in section 3. Section 4 discusses the results of the three-dimensional simulations.

Numerical model

We consider a stably stratified fluid with density $\rho = \rho_0 + \overline{\rho} + \rho'$. The background density ρ_0 is constant, the stratification is characterized by the mean part $\overline{\rho}(z)$ whereas the density fluctuations in the fluid are ρ'. In the numerical simulations we use the temperature, $\theta = \theta_0 + \Theta + \theta'$, with the mean Θ as dependent variable (linearized equation of state) instead of the density:

$$\frac{\Theta + \theta' - \theta_0}{\theta_0} = -\frac{\overline{\rho} + \rho' - \rho_0}{\rho_0}; \quad \frac{\theta'}{\theta_0} = -\frac{\rho'}{\rho_0}. \tag{1}$$

The Boussinesq approximation is assumed and the equations are transformed to dimensionless form with constant reference values for time, length, velocity, temperature, and pressure, respectively:

$$t_{ref} = \frac{H}{\Delta U}, L_{ref} = H, U_{ref} = \Delta U, \theta_{ref} = \Delta\Theta, \quad \text{and} \quad P_{ref} = \Delta U^2 \rho_0, \tag{2}$$

where ΔU and $\Delta\Theta$ are the velocity and temperature differences across the vertical depth H. The bulk Richardson number is defined by:

$$Ri = \frac{g\Delta\Theta H}{\theta_0 \Delta U^2}. \tag{3}$$

The governing equations are then the conservation laws for mass, momentum and temperature

$$\frac{\partial}{\partial \overline{x}^d}\left(\rho_0 V G^{dq} u_q\right) = 0, \tag{4}$$

$$\frac{\partial}{\partial t}\left(V u_i\right) + \frac{\partial}{\partial \overline{x}^d}\left(V G^{dq} u_q u_i\right) = -\frac{\partial}{\partial \overline{x}^g}\left(V G^{gi} p\right) - \frac{\partial}{\partial \overline{x}^d}\left(G^{ds}\left(V F_{is}\right)\right) + Ri V \theta' \delta_{3i}, \tag{5}$$

$$\frac{\partial}{\partial t}\left(V\theta'\right) + \frac{\partial}{\partial \overline{x}^d}\left(V G^{dq} u_q \theta'\right) + V u_3 \frac{d\Theta}{dx_3} = -\frac{\partial}{\partial \overline{x}^d}\left(G^{dr}\left(V Q_r\right)\right). \tag{6}$$

The Cartesian velocity components $u_i = (u, v, w)$ and the temperature perturbation θ' are computed on a terrain following coordinate system in which the curvilinear coordinates $(\overline{x}, \overline{y}, \overline{z})$ are related to Cartesian coordinates (x, y, z) according to

$$\overline{x} = x, \quad \overline{y} = y \quad \text{and} \quad \overline{z} = \eta(x, y, z) = H\frac{(z-h)}{(H-h)}. \tag{7}$$

The Jacobian of the transformation $G^{ij} = \partial \overline{x}_i / \partial x_j$ is $V = (det\, G^{ij})^{-1}$ and $h(x, y)$ is the prescribed height of the bottom surface. For details of the numerical implementation of this coordinate transformation see Krettenauer and Schumann [4]. The diffusive fluxes in Eq. 5 and Eq. 6 are

$$V F_{ij} = -\rho K_M V D_{ij}, \quad V Q_i = -\rho K_H \frac{\partial}{\partial \overline{x}^r}\left(V G^{ri} \theta'\right), \tag{8}$$

where $K_M = 1/Re + \nu_{turb}$ and $K_H = 1/ReSc + \nu_{turb}/Sc_{turb}$. The Reynolds and Schmidt numbers are defined by $Re = \Delta U H/\nu$ and $Sc = \nu/\nu_\rho$. The turbulent viscosity is determined as a function of the local Richardson number as suggested by Mason and Derbyshire [7]:

$$\nu_{turb} = \begin{cases} \Lambda^2 |S - \overline{S}| \sqrt{1 - \frac{Ri}{Ri_c}}, & \text{when} \quad Ri < Ri_c = 1 \\ 0 & \text{otherwise,} \end{cases} \tag{9}$$

where S is the deformation tensor in terrain following coordinates

$$S = \sqrt{0.5 D_{ij} D_{ij}}, \quad D_{ij} = \frac{1}{V}\frac{\partial}{\partial \overline{x}^r}\left(V G^{rj} u_i + V G^{ri} u_j\right). \tag{10}$$

The mean shear $\overline{S} = \Delta U/H$ is subtracted from the local deformation S in Eq. 9 so that the turbulent diffusivity is zero in the unperturbed mean flow and nonzero only in the 'turbulent' regions with strong deviations from the linear profile. The mixing scale is related to the grid spacings as $\Lambda = 0.1\left(\Delta x + \Delta y + \Delta z\right)/3$. The initial velocity field and the mean temperature field are given by:

$$u(z) = \frac{\Delta U}{H}(z - 0.5H), \Theta(z) = \theta_0 \left\{1 + \frac{\Delta\Theta}{\theta_0}\frac{(z - 0.5H)}{H}\right\}. \quad (11)$$

At the beginning, the perturbations are set to zero or small random fluctuations are prescribed. The computational domain covers one wavelength of the surface undulation, and cyclic boundary conditions in the x-direction are used. The boundary conditions in the cross-stream (y-) direction are also periodic. Since we are not interested in resolving the viscous surface layers of the laboratory model, the boundary conditions

$$\frac{\partial\theta'}{\partial z} = 0, \quad \frac{\partial u}{\partial z} = \frac{\Delta U}{H}, \quad \frac{\partial v}{\partial z} = 0, \quad \frac{\partial VF_{13}}{\partial z} = 0 \quad (12)$$

are used at the upper and lower surfaces. The normal velocity is zero at the wall boundaries.

Comparison with measurements for a weakly nonlinear shear flow

In this chapter, we compare the results of a two-dimensional numerical simulation with the measurements of Thorpe [13] who observed the internal gravity-wave critical-layer interaction in the laboratory. In this case, the mean velocity is zero and an uniform shear is induced initially. In the experiment, the lower undulated surface, consisting of sixteen sinusoidal waves, excites the internal gravity waves with zero phase speed in the shear flow. We compare our results with the observations shown in Fig. 4 of Thorpe [13], when the tube is returned into the horizontal position after the time t_α, when the shear flow is no longer accelerated. Its strength depends on the angle α, the time of tilting t_α and the Brunt-Väisälä frequency $N = 2.06s^{-1}$ according to $\Delta U/H = N^2 t_\alpha \sin\alpha$ [12].

The sixteen corrugated waves are replaced by one wave in the computation and cyclic boundary conditions in the horizontal direction. Therefore, the horizontal length of the model domain is $\lambda = 1.5625H$ with $H = 0.16m$. The number of grid points is (200x128). Further parameters supported by the experiment are the amplitude of the wave $\delta = 0.03125H$, and the angle and time of tilting of the tube, $\alpha = 7.1\,^\circ$. and $t_\alpha = 3.75s$, respectively, implying $\Delta U = 0.34m/s$. The mean density profile is assumed to be linear with the constant gradient $\Delta\Theta/H = N^2\theta_0/g$. The corresponding Richardson number is $Ri \approx 1.1$. The initial velocity distribution is prescribed according to Eq. 11 and the temperature field θ' is zero. The viscosity is constant, the turbulent viscosity is set to zero in this simulation.

In the observations, layers of constant density were marked by adding dye. These layers have a certain thickness depending on the experimental set-up. The deformation of these black and white regions illustrates the wave propagation with time. For a quantitative comparison with the measurements, we plot the contour lines of the temperature field with a constant increment $\Delta\theta = 0.0032\Delta\Theta$ in such a way that the thickness and the position of the areas

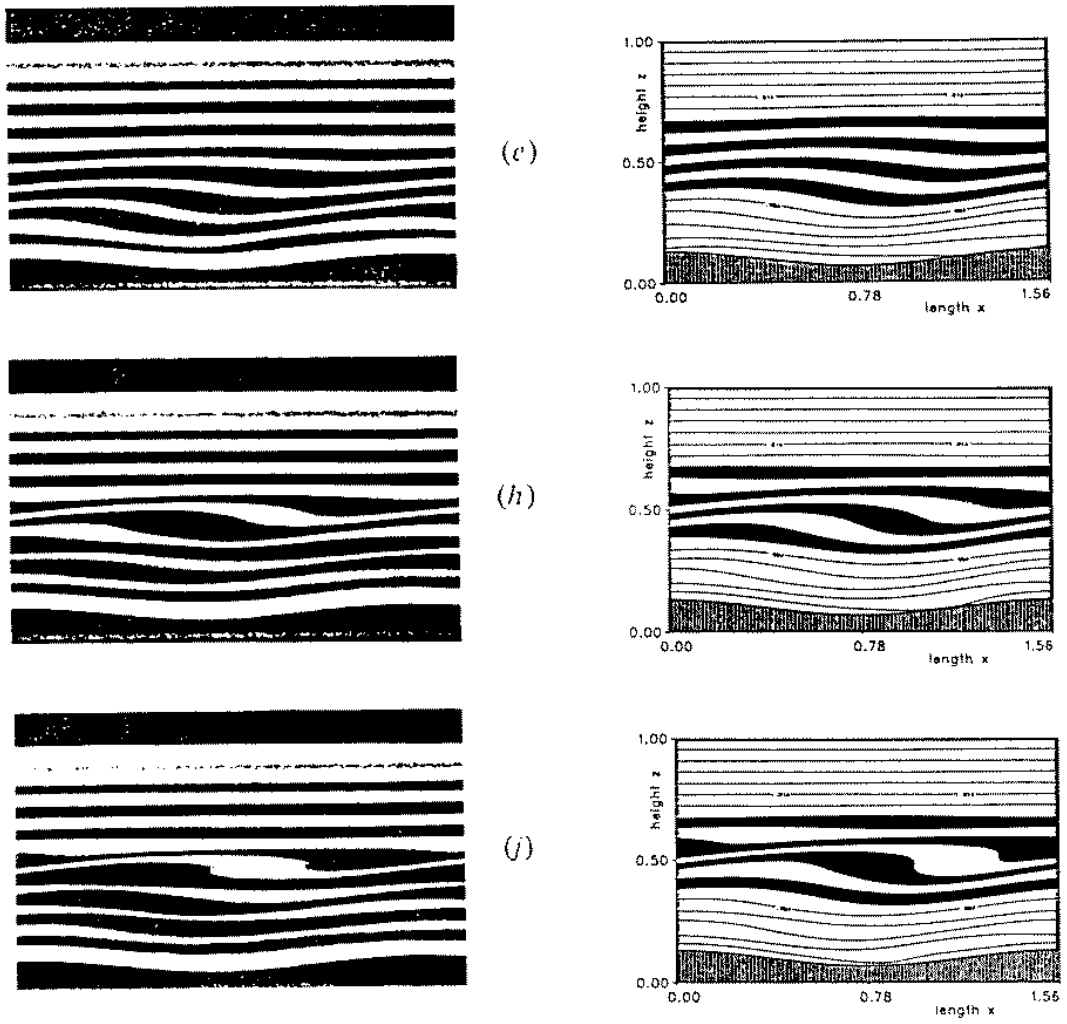

Fig. 1. Comparison with the observations of Thorpe (1981). Left side: experimental results at $t = 4.5s$, $t = 7.9s$, and $t = 10.2s$. Right side: Results of the numerical simulation at corresponding times. The length and height are in units of H.

between adjacent contour lines correspond to the black and white layers documented in the photographs of the observations. The most interesting areas in the middle of the numerical domain are also made black in Figure 1.

At the beginning, the lines of constant temperature are horizontal, i.e. colder (heavier) fluid is lying in the trough and the fluid gets warmer (lighter) with increasing height. The mean flow is towards the left near the surface and towards the right at the top boundary. The overall features of the flow evolution in the laboratory and in the numerical simulation are obviously similar. The sinusoidal corrugations at the bottom surface excite internal gravity waves that propagate vertically towards the critical level (Figure 1(e)). The amplitude of the waves increases with height but falls to zero at the critical level. No wavy motion is found above this level which acts as an absorber

whereby momentum is transfered to the mean flow causing an advection in the positive x-direction. Regions of reduced vertical temperature (density) gradients (characterized by thickening of the marked layers) are mainly found above the trough (Figure 1(h)). Because of the reduced gradients, the local Richardson number drops and these regions become convectively (gravitationally) unstable, where the advection puts colder (heavier) fluid over warmer (lighter) fluid, which finally leads to the wave breaking. Between these sites of instability the vertical gradient is enhanced and the black and white areas over the crest become thinner, a structure similar to that found for Kelvin-Helmholtz instability.

A slight difference can be seen between the observed and the computed position of the unstable region. In the computations overturning occurs further to the right and a more unstable region is visible also on the left side. This may be possibly caused by differences in the shear profile because we do not know the details of the transition from the tilted to the non-tilted tube position. Tests have shown that the acceleration of the mean flow depends very much on the Reynolds number. The lower the Reynolds number the weaker is the transfer of momentum to the mean flow and the smaller the advection causing the breaking. Although we have not used the same boundary conditions as in the experiment (no friction) excellent agreement with the observed flow patterns was obtained. Obviously, the viscous friction at the top and bottom surface is of minor importance in this case. The comparison shows that the model reproduces the weakly nonlinear interaction of a gravity wave with the critical level well.

Breaking of internal gravity waves

Based on the test presented in the former section (and comparisons to linear solutions, to be published elsewhere), we apply the code to the three-dimensional interaction of nonlinear internal gravity waves with the critical layer and the breakdown to turbulence. The domain size in units of H is $(0, 1.5625) \times (0, 0.3125) \times (0, 1)$. The characteristic length scale of the expected structures caused by the breaking is of the order of the thickness of the resulting mixed layer. This scale is essentially less than a quarter of H. Thus, the lateral domain size of $\lambda/5 \approx H/3$ seems to be large enough to allow a well resolved turbulent motion. The finite difference grid is uniform and isotropic with (150x30x96) nodes.

The reference scales of the simulations are the height $H = 0.16m$, the velocity scale $\Delta U = 0.3147m/s$, and the temperature scale $\Delta\Theta/\theta_0 = 0.0692$, which gives a bulk Richardson number of 1.1 at the beginning of the simulations. We present the results of two runs: first, a DNS with constant eddy viscosities K_M and K_H ($\nu_{turb} = 0$, Re=20000, Sc=500) and the zero initial temperature field, and secondly, a LES where the eddy viscosities are calculated by means of Eq. 9, $Sc_{turb} = 1$, and the molecular viscosity is zero. In the LES, the initial

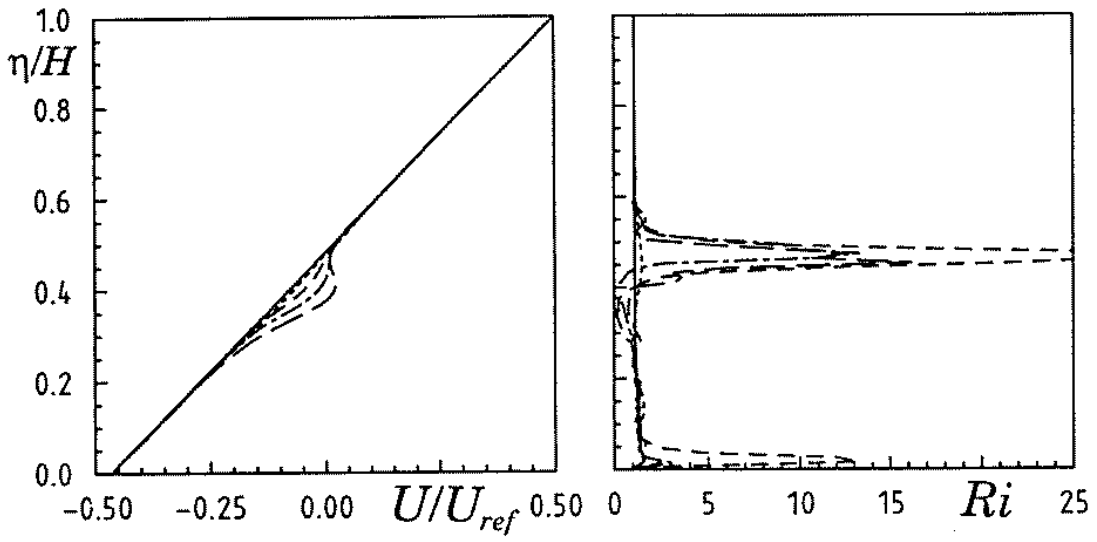

Fig. 2. Profiles of the mean horizontal velocity and Richardson number at five different times for the DNS. The times are $t = 0$ ———, $t = 6t_{ref}$ - - - -, $t = 12t_{ref}$ - - -, $t = 24t_{ref}$ - · -, $t = 40t_{ref}$ — — .

temperature field is disturbed by small random fluctuations with a variance $\sqrt{\overline{\theta'^2}} = 0.001\Delta\Theta$. The time step is $\Delta t = 0.005t_{ref}$ and the simulations run until $t = 40t_{ref}$.

Figure 2 shows the horizontally (at $\eta = const.$) averaged profiles of the u-velocity and the local Richardson number at five different times for the DNS. Below the critical level $\eta \approx 0.5H$ the mean velocity increases in time. While the increase up to about $t = 20t_{ref}$ is similar in the DNS and the LES, the final speed-up at $t = 40t_{ref}$ is $0.011\Delta U$ in the DNS and only $0.007\Delta U$ in the LES. The layer directly influenced by the momentum transfer between the wave and the mean flow has a thickness of about H/4. We expect that this layer thickness depends on Ri and possibly on δ/H. Just below the critical level the Richardson number becomes much larger compared to its initial value due to the decreasing shear and the increasing stratification at this altitude. Below the level of maximum acceleration ($\eta \approx 0.4H$) the shear is large and Ri drops below the critical value Ri_c and becomes even negative indicating a layer with smaller or negative temperature gradients. Indeed, the temperature fluctuations (not shown) are positive below and negative above this level and cause a convectively unstable layer. This suggests that mixing is mainly driven by the wave induced convective instability and not by a Kelvin-Helmholtz instability.

Figure 3 shows the profiles of the horizontally averaged kinetic energy $E = 0.5\left(\overline{u'^2} + \overline{v'^2} + \overline{w'^2}\right)$ at the same instances as in Figure 2 for the DNS and LES. Despite the two different regimes of breaking (see Figure 5) the magnitude of the variances is nearly the same in the two cases. The kinetic

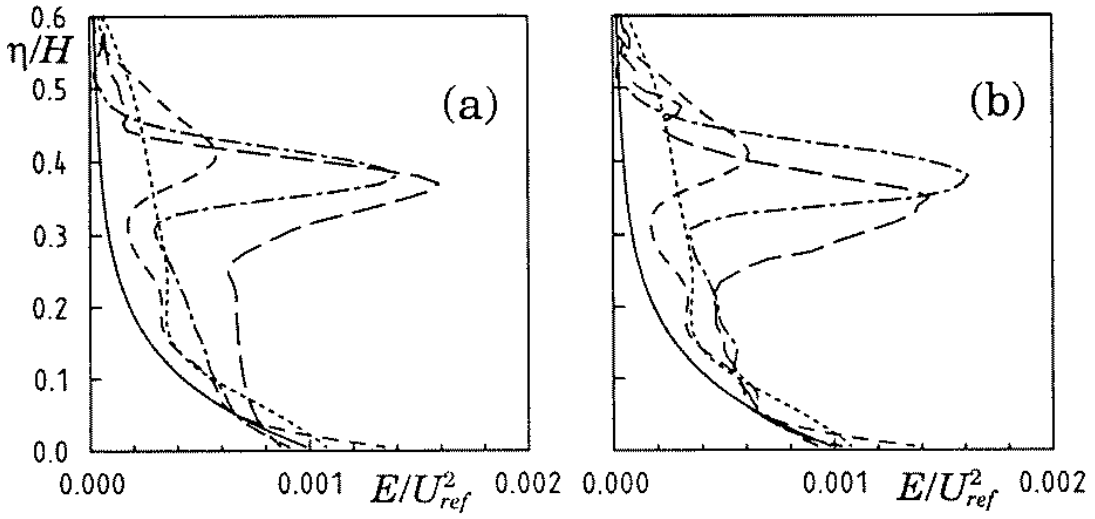

Fig. 3. Profiles of the horizontally averaged kinetic energy $E = 0.5\left(\overline{u'^2} + \overline{v'^2} + \overline{w'^2}\right)$ for the DNS (a) and the LES (b). Line coding as in Fig. 2.

energy E exhibits two maxima, one near the surface and one below the critical level. The first one is caused kinematically by the flow over the wavy terrain and is mainly due to the contribution of the w-variance. The second extreme value is produced dynamically by the breakdown of the vertically propagating wave and comprises contributions of the u- and w-variance. The v-variance is different from zero only in the disturbed case and is one order of magnitude smaller than $\overline{u'^2}$. Hence, the flow remains essentially two-dimensional in the DNS case but becomes turbulent and three-dimensional in the LES case. Above the critical level, up to $0.6H$, the variances start to grow slightly in an initial period but return to zero soon. This illustrates the inhibiting effect of the critical layer on the dynamics. The temporal evolution of the variance profiles is different for the two cases. The u-variances increase at the same rate up to about $24t_{ref}$ in both cases, but the magnitude of $\overline{u'^2}$ stays nearly constant in the uniform viscosity case while it decreases strongly in the disturbed case. Obviously, the three-dimensional mixing is more effective and prevents a further acceleration of the mean flow and leads to a restratification of the fluid which limits further mixing. The ongoing growth of energy E in the DNS is caused by the increasing w-variance due to the continuous build up of unstable regions by rolling motions in the mixed layer. If we look at the vertical position of this layer, we observe a sinking motion with time, which is stronger for the LES case. Such sinking of thin turbulent layers has also been observed by radar in the free atmosphere [10].

One of the most important consequences of the absorption of a wave at the critical level is the acceleration of the mean flow (see Figure 2). This acceleration requires a vertical gradient of the shear stress, because $\partial u/\partial t \sim$

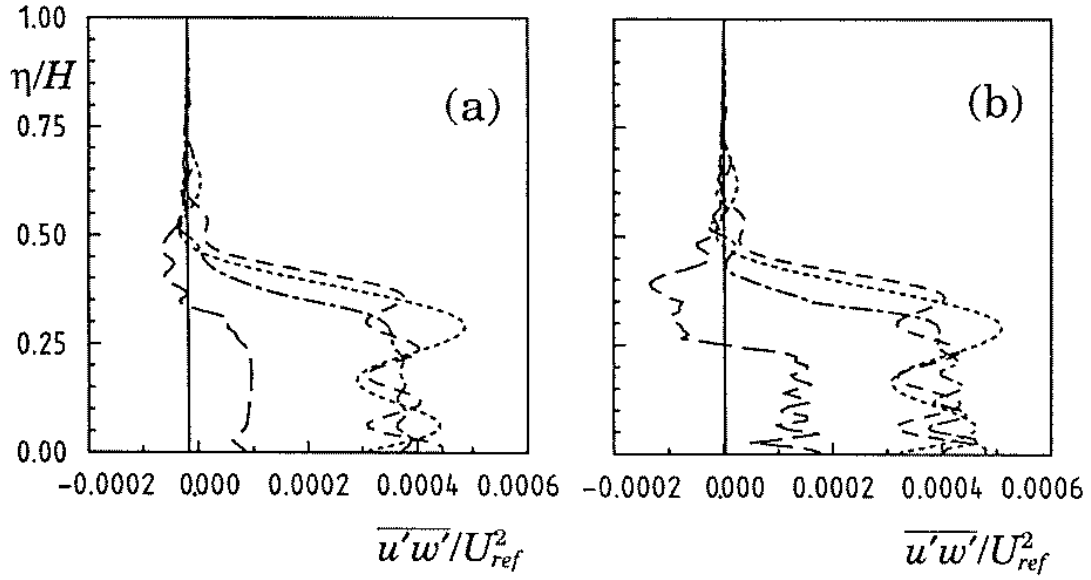

Fig. 4. Profiles of the momentum flux $\overline{u'w'}$ for the DNS (a) and the LES (b). Line coding as in Fig. 2.

$-\partial\overline{u'w'}/\partial z$. Idealized waves with infinite extent have an uniform momentum flux and the gradient is zero, i.e. on average the fluid is never forced. In our simulations, the $\overline{u'w'}$-profiles manifest a strong vertical structure (Figure 4). Initially, the vertical flux of horizontal momentum is constant (zero for the disturbed, slightly negative for the uniform viscosity case). At $t = 6t_{ref}$, the $\overline{u'w'}$-profile exhibits vertically a wavelike structure. Its amplitude increases with altitude but strongly decreases to the initial value just below the critical level. Between $z \approx 0.3H$ and $z \approx 0.5H$ the gradient is negative and large and causes the strong acceleration of the mean flow. Due to the wavelike structure of the profiles, below this region other layers exist with an accelerated or decelerated motion. At $t > 12t_{ref}$, the number of waves is increased and at $t > 24t_{ref}$ the shear stress is nearly uniform below the critical level. After the breaking event, the shear stress is heavily reduced and becomes negative in the formerly forced region. The reduction is much stronger in the LES than in the DNS. This means the turbulent mixing (which now actually includes the third dimension) in the LES is much more effective than the more or less two-dimensional regime of the DNS.

Figure 5 shows contour lines of the temperature field $\theta' + \Theta(z)$ at a late time for the DNS and LES, respectively. In order to make the important effects better visible, four intervals between constant temperature contours have been marked black. From a sequence of those pictures at various times, we find that the temporal development of the wave structure up to the time $t = 18t_{ref}$ is similar to the results shown in Figure 1. The flow over the wavy surface excites internal gravity waves which propagate vertically upward and generate regions

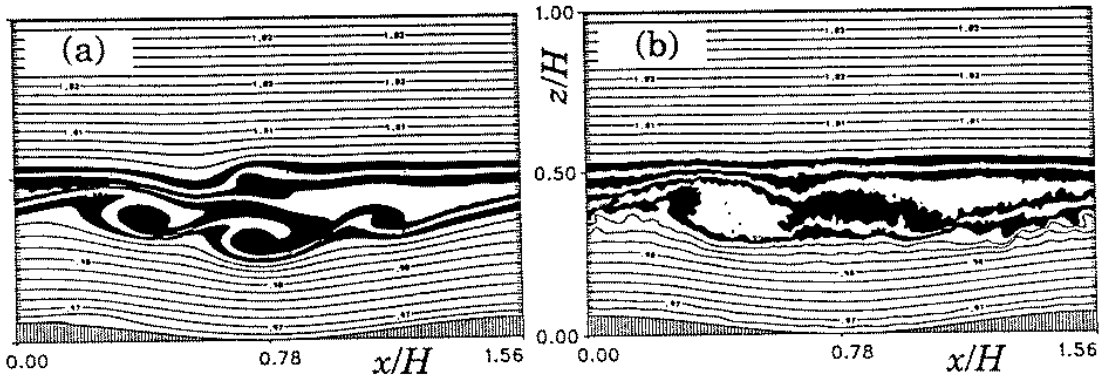

Fig. 5. Contour lines of $\theta' + \Theta$ at $t = 40_{ref}$ for the DNS (a) and the LES (b).

of reduced stability (over the trough) as well as regions where the contour lines are crowded (the braids over the crest). Above the critical level, no or very reduced wavy motion is observed. When we measure the difference of the extreme values of a contour line, we realize that this amplitude increases as a function of height and becomes nearly 3δ. This indicates that the wavy motion at the critical level experiences a long lasting excitation from the surface wave. At other levels the longitudinal motion of the fluid prevents such an excitation. The first overturning occurs at about $t = 14t_{ref}$. Then the flow development becomes different for the DNS and LES. The uniform viscosity case shows a smoothly breaking regime, which consists of the repeated rolling-up of density surfaces whereas the turbulent viscosity case leads to a fully turbulent mixed layer below the critical level.

In the DNS, we see no indication of the onset of secondary, smaller-scale or three-dimensional instabilities, neither in the statically unstable cores, nor in the braids, where a shear driven instability would be possible. Here, the main characteristic is the continuous generation of overturning waves induced by shear and the primary waves. After the breakdown of the first wave at earlier times (between $t = 30$ and $t = 36t_{ref}$), we find a second unstable region which itself creates a smaller wave with growing amplitude. In the LES, the heavier fluid breaks immediately by falling down and a strong turbulent mixing occurs in the unstable regions. Between $t = 30$ and $t = 36t_{ref}$ there is also a tendency to build up a secondary wave structure but this is destroyed quickly by the mixing. At the end of the simulation we find large areas of reduced vertical density gradients, but only small portions of the fluid are convectively unstably stratified.

Conclusions

The nonlinear interaction of an internal gravity wave with the critical level and the generation of a turbulent mixed layer has been investigated by means

of DNS and LES. The turbulent viscosity is assumed to be proportional to the fluctuation of the local shear and is a function of the Richardson number. The flow structure in the DNS remains essentially two-dimensional. The mixing takes place as a process of repeated rolling-up of density surfaces so that the flow shows permanently overturning waves which generate vertical motions in a quasi periodic manner without real turbulence. Because of the three-dimensional initial disturbances and the weaker effective diffusivity, the overturning waves in the LES produce turbulent mixing which is more efficient than the two-dimensional counterpart. In both cases, no Kelvin-Helmholtz instability is observed. Further studies will be devoted to the investigation of the effects of the bulk Richardson number, the amplitude of the surface wave and the characteristics of the resulting turbulence.

Acknowledgements

This work has been supported by the Deutsche Forschungsgemeinschaft.

References

1. Booker, J. R. and Bretherton, F. P., The critical layer for internal gravity waves in a shear flow. *J. Fluid Mech.* **27** (1967) 513-539.
2. Delesi, D. P. and Dunkerton, T. J., Laboratory observations of gravity wave critical-layer flows. *Pure Appl. Geophys.* **130** (1989) 445-461.
3. Koop, C. G. and McGee, B., Measurements of internal gravity waves in a continiously stratified shear flow. *J. Fluid Mech.* **172** (1986) 453-480.
4. Krettenauer, K. and Schumann, U., Numerical simulation of turbulent convection over wavy terrain. *J. Fluid Mech.* **237** (1992) 261-299.
5. Nappo, C. J. and Chimonas, G., Wave exchange between the ground surface and a boundary-layer critical level. *J. Atmos. Sciences* **49** (1992) 1075-1091.
6. Nastrom, G. D. and Eaton, F. D., The coupling of gravity waves and turbulence at White Sands, New Mexico, from VHF radar observations. *J. Appl. Meteorol.* **32** (1993) 81-87.
7. Mason, P.J. and Derbyshire, S. H., Large-eddy simulation of the stably stratified atmospheric boundary layer. *Bound.-Layer Meteorol.* **53** (1990) 117-162.
8. Merrill, J. T. and Grant, J. R., A gravity wave - critical level encounter observed in the atmosphere. *J. Geophys. Res.* **84** (1979) 6315-6320.
9. Pao, Y. and Goldburg, A. (eds.), *Clear air turbulence and its detection.* Plenum Press, New York, 1969.
10. Sato, K. and Woodman, R. F., Fine altitude resolution radar observations of stratospheric layers by the Arecibo 430 MHz radar. *J. Atmos. Sciences* **39** (1982) 2546-2552.
11. Sidi, C., Waves-turbulence coupling. *Coupling Processes in the Lower and Middle Atmosphere* E. V. Thrane et al. (eds.), Kluwer Amsterdam (1993) 291-304.
12. Thorpe, S. A., A method of producing a shear flow in a stratified fluid. *J. Fluid Mech.* **32** (1968) 693-704.
13. Thorpe, S. A., An experimental study of critical layers. *J. Fluid Mech.* **103** (1981) 321-344.